# Improved Geiger-Nuttall law for one-proton and two-proton radioactivity*

Zhipeng Han (韩志鹏) Niu Wan (万牛)†

School of Physics and Optoelectronics, South China University of Technology, Guangzhou 510641, China

**Abstract:** Proton radioactivity, a rare decay mode occurring in proton-rich nuclei beyond the proton drip line, provides valuable insights into nuclear structure, nuclear stability, and the limits of nuclear existence. Building upon the Geiger–Nuttall (GN) law and recent developments in one-proton and two-proton radioactivity systematics, this work proposes an improved GN law that explicitly separates the effects of the daughter-nucleus charge $Z_d$ and the orbital angular momentum $l$. Previous empirical formulas typically couple or add these two contributions, despite their fundamentally different physical origins—the long-range Coulomb interaction and the relatively shorter-range centrifugal potential. By introducing an additional parameter to independently scale the $l$-dependent contribution, we quantify their separate roles on the decay half-life. Using experimental data from 44 proton emitters and available two-proton emitters, we determine the optimal parameter sets for both one-proton and two-proton radioactivity. The improved GN law yields a smaller standard deviation $\sigma$=0.357 for one-proton emission and reproduces experimental two-proton radioactive half-lives within one order of magnitude. The resulting law provides enhanced predictive power and a physically transparent interpretation of Coulomb and centrifugal contributions, offering reliable theoretical support for future studies and experimental searches of exotic proton-rich nuclei.

**Keywords:** proton radioactivity, Geiger-Nuttall law, decay half-life

**DOI:** **CSTR:**



## I. INTRODUCTION

Due to the rapid development of radioactive beam facilities, the studies on nuclei around the proton drip line have attracted more and more attention in modern nuclear research. In this region with extremely proton-rich nuclei, one-proton and two-proton radioactivity provide unique insights into nuclear structure, single-particle configurations, pairing correlations, and the limits of nuclear binding. Proton radioactivity was first observed in 1970 in the isomeric state of $^{53}$Co [1, 2] and since then more than forty proton emitters have been identified between $Z = 53$ and $Z = 83$ [3−9]. Similar to $\alpha$ decay[10, 11], proton emission is also described as a quantum tunneling process, where an unbound proton penetrates the composite barrier formed by the Coulomb and centrifugal potentials, resulting in a strong sensitivity of the decay half-life $T_{1/2}$ to both the decay energy $Q_p$ and the orbital angular momentum $l$ carried by the emitted proton.

There are many microscopic descriptions based on the semiclassical Wentzel-Kramers-Brillouin (WKB) approach which provide valuable insights into the decay mechanism of proton radioactivity, such as the single-particle Schrödinger equation with a Woods-Saxon potential [12−14] or Jeukenne, Lejeune and Mahaux (JLM) potential [15], the single-folding model (SFM) [5], the Gamow-like model (GLM) [16, 17], the unified fission model (UFM) [18, 19], the Coulomb and proximity potential model (CPPM) [8, 20−22], the relativistic mean-filed theory [23−30], and the density-dependent cluster model (DDCM) [31−34]. These approaches usually require detailed nuclear-structure inputs such as explicit interactions. As a result, empirical formulas inspired by the classical Geiger–Nuttall (GN) law can be an essential tool for describing proton radioactivity in a simple but physically meaningful manner. Early GN-type extensions for proton radioactivity also emphasized the correlation between $\log_{10}T_{1/2}$ and $Q_p^{-1/2}$, but modified by the Coulomb parameter or angular-momentum hindrance. Delion et al. [4] introduced an empirical linear relation for reduced half-lives of proton radioactivity, while Brown-type formulas were adapted to incorporate the influence of the daughter charge number $Z_d$, yielding a dependence on $Z_d^{0.6}$. Based on these formulas, subsequent improvements further explicitly introduced the dependence on orbital angular momentum $l$. For example, Budaca et al. [35] divided the experimental data by angular-mo-

Received 10 December 2025; Accepted 24 February 2026

* This work was supported by the National Natural Science Foundation of China (Grants No. 12205105), by the Fundamental Research Funds for the Central Universities (Grant No. 2024ZYGXZR058) and the startup funding of South China University of Technology

† E-mail: wanniu@scut.edu.cn

mentum quantum numbers $l$ into different groups with dependence on $Z_d^{0.73}$ and $Z_d^{0.85}$, respectively, while Sreeja et al. [36] unified the $l$-dependence into their formula with dependence on $Z_d^{0.8}$. Both empirical relations successfully reproduced the decay half-lives of known proton emitters with reasonable accuracy. Recently, a new GN (NGN) law is further formulated for proton radioactivity [37], where the two-parameter expression

$$\log_{10} T_{1/2} = a(Z_d^{0.8} + l)Q_p^{-1/2} + b, \quad (1)$$

captures the combined effects of Coulomb repulsion and angular-momentum hindrance in a compact form. Fitting experimental data from 44 proton emitters, they obtained a standard deviation of $\sigma = 0.397$, outperforming earlier GN-type relations as well as several microscopic models including the modified Gamow-like model and the Coulomb–proximity potential model.

For two-proton radioactivity, a wide variety of theoretical approaches have been developed, including three-body decay [38−42], diproton models [43], Gamow-like model [20, 44], and macroscopic descriptions such as the effective liquid drop model (ELDM) [45, 46] and the generalized liquid-drop model (GLDM) [47]. Meanwhile, the empirical extensions of the GN law have also proven highly effective. Sreeja et al. [48] proposed a four-parameter empirical formula based on ELDM systematics, while the GLDM is further applied to the study of two-proton radioactivity [47]. Based on the concept shown in Eq. (1) for one-proton radioactivity, the NGN law is further extended for two-proton emissions [49] with the angular-momentum term determined as $l^{0.25}$ through minimum-standard-deviation fitting. Their unified two-parameter law reproduces the measured half-lives of experimental two-proton emitters such as $^{19}$Mg, $^{45}$Fe, $^{48}$Ni, $^{54}$Zn, $^{67}$Kr, and provides predictions consistent with ELDM, GLDM, and the four-parameter formula.

In previous studies such as the NGN formulas given in Eq. (1) for both one-proton and two-proton radioactivity, the Coulomb and centrifugal contributions are usually treated as a single additive quantity $Z_d^{0.8} + l$, implicitly assuming similar scaling behavior for the two potentials. In reality, these two components have distinct physical origins and radial dependencies. In Fig. 1, a sketch is given to explicitly demonstrate the difference between the Coulomb and centrifugal potentials by taking one-proton emitter $^{151}$Lu and two-proton candidate $^{57}$Ga as examples. The Coulomb potential ($\propto 1/R$) arises from the long-range electrostatic repulsion dependent on the daughter-nucleus charge number $Z_d$. It varies smoothly with the relative distance $R$ and dominates in the outer tunneling region. In contrast, the centrifugal potential ($\propto 1/R^2$) is a relatively shorter-range quantum effect dependent on the orbital angular momentum $l$. It decreases sharply with the

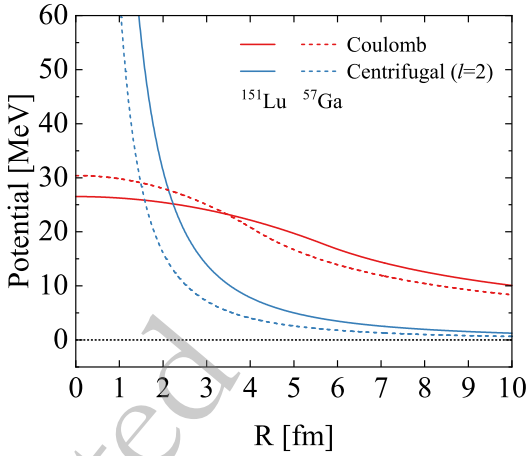


**Fig. 1.** (color online) Sketch of the Coulomb and centrifugal potentials by taking one-proton emitter $^{151}$Lu and two-proton candidate $^{57}$Ga as examples.

relative distance and provides contributions mainly in the inner barrier region. Though there exist differences between these two potentials, above single additive quantity $Z_d^{0.8} + l$ is usually employed to evaluate their common contributions to the decay half-lives within the GN law. Hence, it is of particular interest to separate this additive term to quantify their distinct contributions to the decay half-lives.

Motivated by the recent successful concept from the NGN law in Eq. (1), we propose an improved GN law in which the Coulomb and centrifugal terms are explicitly separated with an independent separation factor introduced for the angular-momentum term. This approach allows the long-range Coulomb and relatively shorter-range centrifugal contributions to be optimized independently and evaluated quantitatively. By fitting the experimental data for one-proton and two-proton emitters, we extract optimal parameters, analyze the relative contribution of each potential component, and demonstrate that the improved formulation yields reduced standard deviations and more physically transparent systematics. The resulting empirical relation offers a simple yet powerful tool for studying and predicting proton and two-proton radioactivity near the limits of nuclear stability. This paper is organized as follows. In section II we give the details about the framework of the improved GN law. The corresponding results for both one-proton and two-proton radioactivity and discussion are given in section III. A summary is given in section IV.

## II. FRAMEWORK

In this section we present the formulation of the improved Geiger-Nuttall (GN) law and describe the procedure used to determine its parameters for both one-proton and two-proton radioactivity. The goal is to construct a compact empirical expression in which the Coulomb and

centrifugal contributions are separated as independent physical terms so that we can study their different effects on the decay half-lives within the GN-type formulas.

Motivated by the classical GN law and recent empirical extensions, we introduce the following improved form to study the decay half-lives for both one-proton and two-proton radioactivity:

$$\log_{10} T_{1/2} = a(Z_d^{\alpha} + bl^{\beta})Q^{-1/2} + c, \tag{2}$$

where $Z_d$ is the charge number of the daughter nucleus, $l$ is the orbital angular momentum carried by the emitted proton(s), $Q$ represents the one-proton or two-proton decay energy $Q_p$ or $Q_{2p}$, and $a$, $b$, $c$, $\alpha$, $\beta$ are parameters to be determined by the least square fitting process. The decay energies $Q_p$ and $Q_{2p}$ are respectively calculated by the mass excesses of the mother nucleus, the daughter nucleus, and the emitted proton(s), which are taken from the AME2016 and NUBASE2016 evaluations [50−52]. The key feature in the above formula is the introduction of the independent coefficient $b$, which allows the centrifugal contribution $l^{\beta}$ to scale separately from the Coulomb term $Z_d^{\alpha}$. This improved formulation therefore enables quantitative separations between the long-range Coulomb potential and the relatively shorter-range centrifugal potential.

The orbital angular momentum $l$ carried by the emitted proton(s) is obtained from spin–parity selection rules. Proton emission must satisfy

$$\boldsymbol{J}_m = \boldsymbol{J}_d + \boldsymbol{J}_p, \quad \pi_m = \pi_d \pi_p (-1)^l. \tag{3}$$

where $\boldsymbol{J}_m$, $\boldsymbol{J}_d$, and $\boldsymbol{J}_p$ are the spins of the mother nucleus, daughter nucleus, and emitted proton(s), respectively, while $\pi_m$, $\pi_d$, $\pi_p$ are their corresponding parities. Following the standard selection rules, the minimum allowed angular momentum is obtained by

$$l_{\min} = \begin{cases} \Delta_j & \text{for even } \Delta_j \text{ and } \pi_p = \pi_d, \\ \Delta_j + 1 & \text{for even } \Delta_j \text{ and } \pi_p \neq \pi_d, \\ \Delta_j & \text{for odd } \Delta_j \text{ and } \pi_p \neq \pi_d, \\ \Delta_j + 1 & \text{for odd } \Delta_j \text{ and } \pi_p = \pi_d, \end{cases} \tag{4}$$

with $\Delta_j = |J_m - J_d - J_p|$. For proton emitters with uncertain spin–parity assignments, we adopt the lowest allowed value $l_{\min}$ consistent with known systematics.

To determine the optimal values of $a$, $b$, $c$, $\alpha$, and $\beta$ in Eq. (2), we perform a least-squares fitting by using the experimental data from 44 proton emitters commonly adopted in recent studies. The standard root-mean-square (rms) deviation $\sigma$ between the calculated and experimental decay half-lives is calculated by

$$\sigma = \sqrt{\frac{1}{N}\sum_{i=1}^{N}\left(\log_{10} T_{1/2}^{\mathrm{calc},i} - \log_{10} T_{1/2}^{\mathrm{expt},i}\right)^2}, \tag{5}$$

where $N$ is the number of the involved data points. The above parameters are adjusted to minimize $\sigma$, and the resulting optimal parameter set will be presented in next section along with detailed discussion.

By separating the Coulomb and centrifugal terms in Eq. (2), we can quantify the relative contribution of each component through the following ratios:

$$R_C = \frac{aZ_d^{\alpha}}{a(Z_d^{\alpha} + bl^{\beta})}, \quad R_l = \frac{abl^{\beta}}{a(Z_d^{\alpha} + bl^{\beta})}. \tag{6}$$

These two quantities provide a physically meaningful measure of how the long-range Coulomb potential and the relatively shorter-range centrifugal potential contribute to the decay half-lives, allowing direct comparison with microscopic expectations.

## III. RESULTS AND DISCUSSION

In this section we present the fitted parameters of the improved GN laws for both one-proton and two-proton radioactivity, where its descriptive ability for these two types of proton radioactivity are also evaluated. Besides, the different contributions of the Coulomb and centrifugal terms are also analyzed.

### A. Fitting for one-proton radioactivity

For one-proton radioactivity, 44 sets of experimental data were used to determine the parameters in Eq. (2), including the ground and isomer states of I, Cs, La, Pr, Eu, Tb, Ho, Tm, Lu, Ta, Re, Ir, Au, Tl, Bi. The experimental data for these one-proton radioactivity such as decay half-lives, spins, and parities are taken from Refs. [6, 16, 17]. The mass excesses of mother and daughter nuclei are mainly taken from Refs. [50, 51], while those for $^{117}$La, $^{140,141}$Ho, $^{144}$Tm, $^{150,151}$Lu, $^{159}$Re, $^{159}$Re$^{m}$, and $^{164}$Ir are taken from Ref. [6].

With these experimental data, the optimal parameters for one-proton radioactivity within the present improved GN law correspond to $a = 1.106$, $b = 0.375$, $c = -27.307$, $\alpha = 0.71$, and $\beta = 1.41$, where the $\alpha$ value for the dependence on the charge number$Z_d$ is consistent with previous calculations of $0.6 \sim 0.85$, indicating the dominant contribution from the Coulomb potential to the decay half-life. Besides, the value of the parameter $b = 0.375$ is less than unity, corresponding to the less contribution from the centrifugal potential, which can be used to quantitatively evaluate the difference of the Coulomb and centrifugal

potentials.

In Table 1, the first four columns provide the one-proton emitters, the decay energies $Q_p$, the angular momentum $l$, and the corresponding experimental decay half-lives. The next four columns list the one-proton radioactive half-lives calculated by other popular models, namely the Gamow-like model, CPPM, UDLP, and the NGN law. The calculated decay half-lives in present work are given in the last column, which are generally consistent with previous calculations. In the last row of Table 1, we list the rms deviations for different approaches, where the present improved GN law achieves the smallest value $\sigma_p = 0.357$. Compared to the original NGN law, the present improved GN law is further improved by $\frac{0.397-0.357}{0.397} = 10.07\%$. This improvement in the standard rms deviation confirms the reasonable separation of the contributions from the Coulomb potential and centrifugal potential in one-proton radioactivity.

In Fig. 2, we plot the experimental one-proton radioactive half-lives and the calculated ones within the present improved GN law. It can be seen that all the data points cluster closely around the red diagonal line. By calculating the Pearson correlation coefficient with $r = \frac{\sum(x_i-\bar{x})(y_i-\bar{y})}{\sqrt{\sum(x_i-\bar{x})^2}\sqrt{\sum(y_i-\bar{y})^2}}$, we obtain a strong Pearson correlation coefficient of $r = 0.9785$, indicating the good agreement between the experimental data and present calculations.

### B. Fitting for two-proton radioactivity

For two-proton radioactivity, available experimental data are very limited. In order to determine the parameters in GN laws, both the experimental data and theoretical calculations are usually employed, including ten experiments of observed two-proton emitters ($^{19}$Mg, $^{45}$Fe, $^{48}$Ni, $^{54}$Zn, $^{67}$Kr) with $l = 0$, and seven predicted results ($^{10}$N, $^{28}$Cl, $^{32}$K, $^{52}$Cu, $^{57}$Ga, $^{60}$As, $^{62}$As) calculated by Goncalves et al. [46] (one case with $l = 1$, four cases with $l = 2$, and two cases with $l = 4$). By fitting these benchmark data, the optimal parameters of the present improved GN law for two-proton radioactivity are $a = 3.112$, $b = 0.680$, $c = -28.565$, $\alpha = 0.69$, and $\beta = 0.23$. Similarly, the $\alpha$ value for two-proton emission is consistent with the previous calculations, while the $b$ value is also less than unity, indicating the reasonable separation of the Coulomb and centrifugal potentials.

In Table 2, we list the involved data of two-proton radioactivity for the fitting process of the present improved GN law. In the first four columns are the two-proton emitters, the decay energies $Q_{2p}$, the angular momentum $l$ carried by the emitted protons, and the corresponding logarithmic benchmark decay half-lives ($\log_{10} T_{1/2}^{\rm expt}$). The next five columns are the theoretical predicted half-lives by the GLDM [47], ELDM [46, 54], the four-parameter empirical formula [48], NGN law [49], and the present

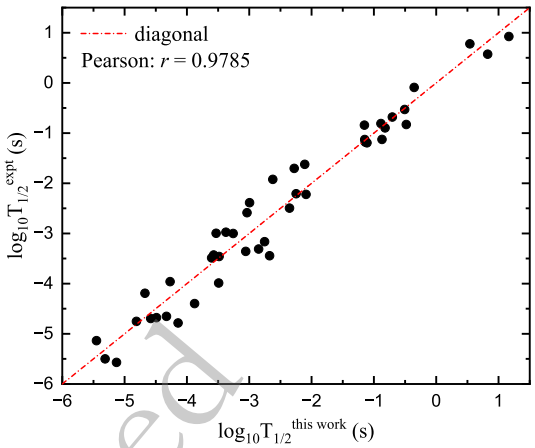


**Fig. 2.** (color online) Correlation between the experimental one-proton radioactive half-lives and those calculated with the present improved GN law.

improved GN law. The last column gives the logarithmic difference between the experimental half-lives and those calculated using the present improved GN law, which is defined as $\Delta = \log_{10} T_{1/2}^{\rm expt} - \log_{10} T_{1/2}^{\rm calc}$. In the last row, we also show the rms deviations $\sigma$ between these theoretical calculations and the experimental data. The present improved GN law yields an rms deviation with $\sigma_{2p} = 0.6728$, which is consistent with previous empirical descriptions of two-proton radioactivity. From the last column we can see that for the true two-proton emitters ($^{19}$Mg, $^{45}$Fe, $^{48}$Ni, $^{54}$Zn, $^{67}$Kr, characterized by $Q_p \le 0$, $Q_{2p} > 0$), most values of the difference $\Delta$ lie between -1 and 1, indicating that the present formula reproduces the corresponding half-lives within one order of magnitude. In particular, for $^{45}$Fe with $Q_{2p} = 1.154$ MeV and $^{48}$Ni with $Q_{2p} = 1.290$ MeV, the differences are $\Delta = 0.061$ and $\Delta = 0.103$, respectively, demonstrating the very good agreement with the experimental data.

We also check the application of the present improved two-proton GN law for the short-lived light two-proton emitters, such as $^{6}$Be, $^{12}$O, $^{16}$Ne with $Q_p > 0$, $Q_{2p} \ge 0$ listed in the lower part of Table 2. It is shown that the differences $\Delta$ are generally larger, especially for $^{6}$Be and $^{16}$Ne, reflecting the additional complexity of these exotic decay modes and possible uncertainties in the benchmark half-lives. The cases of $^{12}$O exhibit a relatively small differences, suggesting that the present improved GN law can also be applicable for the short-lived light two-proton emitters to certain extent when accurate reference data are available. In contrast, the present differences between the benchmark values and those calculated with GLDM, ELDM, and the four-parameter formula all can exceed three orders of magnitude for some two-proton emitters, indicating that further experimental refinement of these half-lives would be valuable.

We also check the global quality of the present GN law with $\log_{10} T_{1/2}^{\rm calc}$ plotted against $\log_{10} T_{1/2}^{\rm expt/ELDM}$ for all

**Table 1.** Comparison of calculated half-lives of one-proton emitters with different theoretical approaches, namely the Gamow-like model [20], the UDLP model [53], the CPPM model [20], the NGN law [37], and our present formula. The symbol "(*m*)" for the mother nucleus indicates an isomeric state. In the last row are the standard rms deviations $\sigma$ for different theoretical calculations with respect to the experimental one-proton radioactive half-lives.

| Nucleus | $Q_p$(MeV) | $l$ | $\log_{10} T_{1/2}(s)$ | | | | | |
|---|---|---|---|---|---|---|---|---|
| | | | Expt. | Gamow-like | CPPM | UDLP | NGN | This work |
| $^{109}$I | 0.830 | 2 | $-3.987^{+0.021}_{-0.022}$ | −3.491 | −3.507 | −3.684 | −3.906 | −3.491 |
| $^{112}$Cs | 0.830 | 2 | $-3.310^{+0.026}_{-0.027}$ | −2.850 | −2.844 | −3.062 | −3.128 | −2.851 |
| $^{113}$Cs | 0.981 | 2 | $-4.752^{+0.010}_{-0.010}$ | −4.811 | −4.796 | −4.899 | −5.302 | −4.812 |
| $^{117}$La | 0.823 [6] | 2 [6] | $-1.623^{+0.038}_{-0.038}$ [6] | −2.110 | −2.072 | −2.350 | −2.368 | −2.111 |
| $^{121}$Pr | 0.901 | 2 | $-1.921^{+0.151}_{-0.234}$ | −2.622 | −2.552 | −2.811 | −2.894 | −2.623 |
| $^{130}$Eu | 1.043 | 2 [6] | $-3.000^{+0.146}_{-0.222}$ | −3.258 | −3.121 | −3.398 | −3.494 | −3.259 |
| $^{131}$Eu | 0.963 | 2 | $-1.699^{+0.044}_{-0.049}$ | −2.279 | −2.141 | −2.458 | −2.477 | −2.280 |
| $^{135}$Tb | 1.193 | 3 | $-2.996^{+0.106}_{-0.141}$ | −3.532 | −3.380 | −3.712 | −3.912 | −3.533 |
| $^{140}$Ho | 1.106 [6] | 3 [6] | $-2.222^{+0.176}_{-0.301}$ [6] | −2.089 | −1.902 | −2.342 | −2.265 | −2.090 |
| $^{141}$Ho$^{m}$ | 1.264 | 0 | $-5.137^{+0.018}_{-0.018}$ | −5.452 | −5.783 | −5.331 | −5.769 | −5.453 |
| $^{141}$Ho | 1.190 | 3 [6] | $-2.387^{+0.010}_{-0.011}$ | −2.995 | −2.811 | −3.220 | −3.335 | −2.996 |
| $^{144}$Tm | 1.725 [6] | 5 [6] | $-5.638^{+0.143}_{-0.216}$ | −5.129 | −5.216 | −4.691 | −5.142 | −5.130 |
| $^{145}$Tm | 1.754 | 5 | $-5.496^{+0.024}_{-0.031}$ | −5.415 | −5.401 | −4.871 | −5.415 | −5.314 |
| $^{146}$Tm$^{m}$ | 0.904 | 0 | $-0.810^{+0.054}_{-0.060}$ | −0.695 | −1.272 | −0.610 | −0.315 | −0.889 |
| $^{146}$Tm$^{m}$ | 1.214 | 5 [6] | $-1.125^{+0.039}_{-0.043}$ | −0.776 | −0.695 | −0.896 | −0.999 | −0.871 |
| $^{147}$Tm | 1.072 | 5 | $0.573^{+0.022}_{-0.023}$ | 0.874 | 1.001 | 0.614 | 0.681 | 0.825 |
| $^{147}$Tm$^{m}$ | 1.133 | 2 | $-3.444^{+0.046}_{-0.051}$ | −3.051 | −2.911 | −2.859 | −2.455 | −2.674 |
| $^{150}$Lu | 1.305 | 2 [6] | $-4.398^{+0.070}_{-0.084}$ | −4.367 | −4.206 | −4.734 | −3.633 | −3.878 |
| $^{150}$Lu | 1.283 [6] | 5 [6] | $-1.194^{+0.273}_{-0.903}$ [6] | −1.044 | −0.931 | −1.113 | −1.199 | −1.111 |
| $^{151}$Lu$^{m}$ | 1.332 [6] | 2 | $-4.782^{+0.018}_{-0.014}$ | −4.582 | −4.582 | −4.327 | −3.899 | −4.117 |
| $^{151}$Lu | 1.255 [6] | 5 [6] | $-0.896^{+0.058}_{-0.066}$ [6] | −0.767 | −0.699 | −0.863 | −0.911 | −0.821 |
| $^{155}$Ta | 1.466 | 5 | $-2.495^{+0.148}_{-0.226}$ | −2.267 | −2.321 | −2.269 | −2.397 | −2.354 |
| $^{156}$Ta$^{m}$ | 1.036 | 2 | $-0.826^{+0.035}_{-0.035}$ | −0.649 | −0.279 | −0.624 | −0.180 | −0.481 |
| $^{156}$Ta | 1.126 | 5 | $0.933^{+0.150}_{-0.136}$ | 1.248 | 1.479 | 0.947 | 1.101 | 1.165 |
| $^{157}$Ta | 0.956 | 0 | $-0.527^{+0.018}_{-0.017}$ | −0.305 | 0.122 | −0.188 | −0.797 | −0.507 |
| $^{159}$Re | 1.816 [6] | 5 [6] | $-4.678^{+0.076}_{-0.092}$ [6] | −4.428 | −4.639 | −4.268 | −4.493 | −4.489 |
| $^{159}$Re$^{m}$ | 1.831 [6] | 5 [6] | $-4.695^{+0.073}_{-0.088}$ [6] | −4.524 | −4.741 | −4.355 | −4.586 | −4.583 |
| $^{160}$Re | 1.286 | 2 | $-3.163^{+0.010}_{-0.010}$ | −3.090 | −2.915 | −2.939 | −2.450 | −2.756 |
| $^{161}$Re | 1.216 | 0 | $-3.357^{+0.001}_{-0.001}$ | −3.152 | −2.953 | −2.895 | −3.277 | −3.058 |
| $^{161}$Re$^{m}$ | 1.336 | 5 | $-0.678^{+0.028}_{-0.028}$ | −0.601 | −0.579 | −0.789 | −0.729 | −0.704 |
| $^{164}$Ir | 1.844 [6] | 5 [6] | $-3.947^{+0.190}_{-0.134}$ [6] | −4.213 | −4.376 | −4.114 | −4.247 | −4.270 |
| $^{165}$Ir$^{m}$ | 1.737 | 5 | $-3.428^{+0.042}_{-0.047}$ | −3.502 | −3.685 | −3.472 | −3.550 | −3.572 |
| $^{166}$Ir | 1.177 | 2 | $-0.842^{+0.081}_{-0.103}$ | −1.294 | −1.036 | −1.303 | −0.801 | −1.153 |
| $^{166}$Ir$^{m}$ | 1.347 | 5 | $-0.090^{+0.025}_{-0.026}$ | −0.215 | −0.136 | −0.475 | −0.344 | −0.354 |
| $^{167}$Ir | 1.087 | 0 | $-1.127^{+0.009}_{-0.009}$ | −0.940 | −0.631 | −0.865 | −1.347 | −1.148 |
| $^{167}$Ir$^{m}$ | 1.262 | 5 | $0.787^{+0.013}_{-0.014}$ | 0.683 | 0.758 | 0.348 | 0.546 | 0.539 |
| $^{170}$Au | 1.487 | 2 | $-3.488^{+0.070}_{-0.081}$ | −3.984 | −3.927 | −3.845 | −3.254 | −3.604 |

Continued on next page

Table 1-continued from previous page

| Nucleus | $Q_p$(MeV) | $l$ | $\log_{10}T_{1/2}(s)$ | | | | | |
|---|---|---|---|---|---|---|---|---|
| | | | Expt. | Gamow-like | CPPM | UDLP | NGN | This work |
| $^{170}$Au$^{m}$ | 1.767 | 5 | $-2.976^{+0.034}_{-0.036}$ | −3.307 | −3.442 | −3.333 | −3.330 | −3.376 |
| $^{171}$Au | 1.464 | 0 | $-4.652^{+0.044}_{-0.049}$ | −4.569 | −4.527 | −4.298 | −4.460 | −4.329 |
| $^{171}$Au$^{m}$ | 1.718 | 5 | $-2.587^{+0.038}_{-0.036}$ | −2.966 | −3.144 | −3.026 | −2.992 | −3.037 |
| $^{176}$Tl | 1.278 | 0 | $-2.208^{+0.137}_{-0.201}$ | −2.133 | −1.909 | −2.059 | −2.361 | −2.249 |
| $^{177}$Tl | 1.172 | 0 | $-1.177^{+0.106}_{-0.142}$ | −0.855 | −0.610 | −0.863 | −1.263 | −1.140 |
| $^{177}$Tl$^{m}$ | 1.979 | 6 | $-3.459^{+0.126}_{-0.176}$ | −3.025 | −3.305 | −3.045 | −3.643 | −3.485 |
| $^{185}$Bi$^{m}$ | 1.625 | 0 | $-4.192^{+0.028}_{-0.031}$ | −4.971 | −5.017 | −4.759 | −4.730 | −4.675 |
| $\sigma$ | | | | 0.501 | 0.472 | 0.427 | 0.397 | 0.357 |

**Table 2.** Comparison of the experimental data for two-proton radioactive nuclei with predictions by different theoretical models, namely GLDM [47], ELDM [46, 54], the four-parameter empirical formula [48], the NGN law [49], and our present formula.

| Nucleus | $Q_{2p}$(MeV) | $l$ | $\log_{10}T_{1/2}$(s) | | | | | | the four-parameter empirical form |
|---|---|---|---|---|---|---|---|---|---|
| | | | Expt. | GLDM | ELDM | Four-Para | NGN | This work | |
| $^{19}$Mg | 0.750 [55] | 0 | $-11.398^{+0.138}_{-0.204}$ [55] | −11.790 | −11.720 | −10.660 | −12.030 | −10.968 | −0.432 |
| $^{45}$Fe | 1.100 [56] | 0 | $-2.398^{+0.261}_{-0.260}$ [56] | −2.230 | | −1.250 | −2.210 | −1.982 | −0.418 |
| | 1.140 [57] | 0 | $-2.071^{+0.244}_{-0.205}$ [57] | −2.710 | | −1.660 | −2.640 | −2.452 | 0.382 |
| | 1.210 [58] | 0 | $-2.425^{+0.029}_{-0.031}$ [58] | −3.500 | | −2.340 | −3.350 | −3.219 | 0.799 |
| | 1.154 [59] | 0 | $-2.552^{+0.132}_{-0.125}$ [59] | −2.870 | −2.430 | −1.810 | −2.790 | −2.611 | 0.061 |
| $^{48}$Ni | 1.350 [59] | 0 | $-2.076^{+0.402}_{-0.778}$ [59] | −3.240 | | −2.130 | −3.130 | −3.206 | 1.126 |
| | 1.290 [60] | 0 | $-2.523^{+0.239}_{-0.222}$ [60] | −2.620 | | −1.610 | −2.590 | −2.623 | 0.103 |
| $^{54}$Zn | 1.480 [61] | 0 | $-2.432^{+0.203}_{-0.137}$ [61] | −2.950 | −2.520 | −1.830 | −2.810 | −3.075 | 0.645 |
| | 1.280 [62] | 0 | $-2.753^{+0.104}_{-0.108}$ [62] | −0.870 | | −0.100 | −1.010 | −1.156 | −1.604 |
| $^{67}$Kr | 1.690 [63] | 0 | $-1.699^{+0.238}_{-0.238}$ [63] | −1.250 | −0.060 | 0.310 | −0.580 | −1.292 | −0.408 |
| $^{10}$N | 1.300 [46] | 1 | | | −17.640 | −20.040 | −18.590 | −18.425 | |
| $^{28}$Cl | 1.965 [46] | 2 | | | −12.950 | −14.520 | −12.460 | −12.414 | |
| $^{32}$K | 2.077 [46] | 2 | | | −12.250 | −13.460 | −11.550 | −11.594 | |
| $^{57}$Ga | 2.047 [46] | 2 | | | −5.300 | −5.220 | −4.140 | −4.626 | |
| $^{62}$As | 0.692 [46] | 2 | | | 14.520 | 13.830 | 14.180 | 14.407 | |
| $^{52}$Cu | 0.772 [46] | 4 | | | 9.360 | 8.620 | 8.740 | 9.165 | |
| $^{60}$As | 3.492 [46] | 4 | | | −8.680 | −10.840 | −8.330 | −9.206 | |
| $\sigma$ | | | | | | 1.0431 | 0.7989 | 0.6728 | |
| $^{6}$Be | 1.371 [64] | 0 | $-20.290^{+0.030}_{-0.028}$ [64] | −19.370 | −19.970 | −21.950 | −23.810 | −24.278 | 3.978 |
| $^{12}$O | 1.638 [65] | 0 | $> -20.198$ [65] | −19.170 | −18.270 | −18.470 | −20.170 | −20.195 | −0.005 |
| | 1.820 [66] | 0 | $-20.943^{+0.426}_{-0.211}$ [66] | −20.940 | | −18.790 | −20.520 | −20.625 | −0.315 |
| | 1.790 [67] | 0 | $-21.103^{+0.190}_{-0.132}$ [67] | −20.100 | | −18.740 | −20.460 | −20.558 | 0.458 |
| | 1.800 [68] | 0 | $-20.160^{+0.079}_{-0.100}$ [68] | −20.120 | | −18.760 | −20.480 | −20.581 | 0.461 |
| $^{16}$Ne | 1.330 [66] | 0 | $-20.642^{+0.301}_{-0.176}$ [66] | −16.450 | | −15.940 | −17.530 | −17.237 | −3.403 |
| | 1.400 [69] | 0 | $-20.382^{+0.196}_{-0.135}$ [69] | −16.630 | −16.600 | −16.160 | −17.770 | −17.524 | −2.856 |



17 data points in Fig. 3. The data points generally distribute closely around the diagonal line, and a Pearson correlation coefficient of $r = 0.9960$ is obtained, confirming an excellent linear correlation between the calculated values and the adopted benchmark data set. This strong correlation, together with the relatively small rms deviation $\sigma_{2p}$,

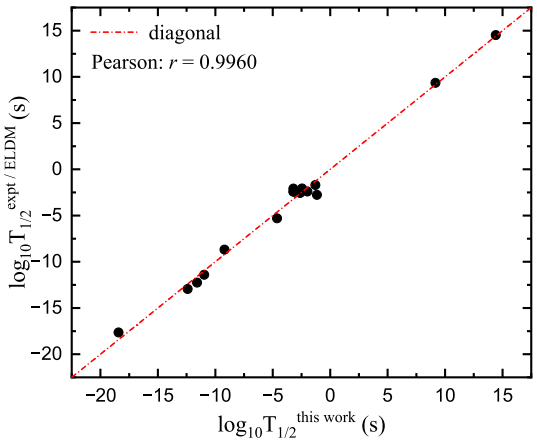


**Fig. 3.** (color online) Comparison between the calculated two-proton radioactive half-lives and the benchmark values from the experimental data and the ELDM results [46].

indicates that the present improved GN law provides a reliable and unified description of both true and short-lived light two-proton emitters. In the future, more realistic two-proton emissions with different angular momenta can be used to further promote the accuracy of present improved GN law.

### C. Coulomb and centrifugal contribution analysis

The explicit separation of the Coulomb and centrifugal terms in Eq. (2) allows a quantitative evaluation of their respective roles in the tunneling process. For each proton emitter, the relative contributions of the two terms to the decay half-lives are assessed using the ratios defined in Eq. (6). The ratios $R_C$ and $R_l$ represent the fractional weights of the Coulomb and centrifugal components in the composite quantity $Z_d^{\alpha}+bl^{\beta}$, and therefore provide a direct measure of the importance of the long-range Coulomb potential and the relatively shorter-range centrifugal potential, respectively.

In Fig. 4 the extracted contribution ratios for all one-proton and two-proton emitters are displayed. Several systematic trends can be observed. From the left two panels for one-proton emission cases, we can see that for low angular momentum one-proton emitters such as with $l = 2$ case, the Coulomb term dominates with the contribution ratios around $R_C \approx 0.95$. This is because the centrifugal potential with low angular momentum is generally much smaller than the Coulomb potential. As $l$ increases, the centrifugal contribution grows rapidly with the centrifugal contribution ratios from $R_l \approx 0.05$ to $R_l \approx 0.15$. This evolution is consistent with the radial dependence of the centrifugal potential. Besides, from the comparison between the NGN calculations and present results, we can see that the present separation between the long-range Coulomb potential and the relatively shorter-range centrifugal potential leads to generally smaller contributions of the centrifugal potential to the decay half-lives, reflecting the fact that the outer Coulomb barrier governs the corresponding tunneling process. Hence the present separation can further improve the prediction accuracy with

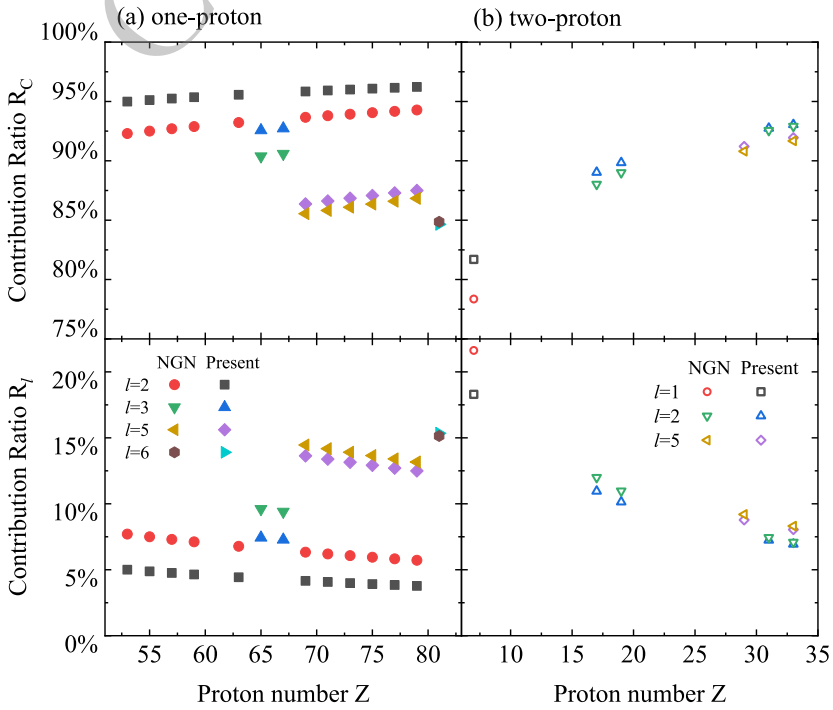


**Fig. 4.** (color online) Coulomb contribution ratios $R_c$ and centrifugal contribution ratios $R_l$ to the decay half-lives for both one-proton (left two panels) and two-proton (right two panels) emissions with different orbital angular momenta.

smaller rms deviation.

Moreover, it can be seen from the left two panels of Fig. 4 that the centrifugal contribution ratios $R_l$ calculated with the NGN law for $l < 6$ cases are systematically larger than those computed by the present work, except the results with $l = 6$ case. This is because the separation factor $b$ is introduced to allow the relative change of the Coulomb and centrifugal contributions. Especially, the centrifugal part with low angular momentum $l$ will contribute less to the decay half-life than that of the NGN law, while it will contribute more with high angular momentum, as exemplified by the case with $l = 6$ in the bottom-left panel of Fig. 4.

From the right two panels of Fig. 4 for two-proton emission cases, we can see a similar behavior that the Coulomb contribution ratios are generally much larger than the centrifugal ones. However, with the angular momentum $l$ increasing, the centrifugal contribution ratios decrease. This is because the two-proton emitters with larger angular momentum $l = 5$ have more than twice proton numbers than those with smaller angular momentum $l = 1$. As a result, the Coulomb contributions are improved much more than the centrifugal contributions, leading to the decreasing extracted $R_l$ values. Hence the contributions of the Coulomb and centrifugal potentials are competitive with each other, and the separation in the present improved GN law provides a more transparent interpretation of proton-radioactivity systematics. Besides, since most known two-proton emitters decay with $l = 0$ transitions are employed in the fitting process, the differences between the present contribution ratios and those extracted using the original NGN law are small. In the future, more experimental data for two-proton emitters with $l > 0$ can be used to check the separating effect on the decay half-life.

### D. Predictions for unmeasured emitters

The predictive capability of the present improved GN law is examined by applying it to the mother nuclei with proton numbers in the range $51 \le Z \le 91$, for which the proton emission is energetically allowed according to the binding energies given in Refs. [50, 51] but whose half-lives remain unmeasured. It should be noted that the nuclear deformation effect is not included in the present work. Considering the general deformations for the proton emitters, the decay energies and the interactions between the emitted protons and the daughter nuclei could be simultaneously affected, leading to crucial impacts on the decay half-lives. In the future, we can further include the deformation effect into the present approach to improve the descriptions for both the measured and unmeasured emitters. The predicted results for the unmeasured emitters within the present framework are summarized in Table 3, where the upper part is for one-proton radioactivity and the lower part is for two-proton radioactivity. The first three columns are the involved mother nuclei, the possible decay energies, and the lowest allowed angular momenta carried by the emitted proton(s). The other columns are the theoretical logarithmic decay half-lives calculated with different approaches as well as present improved GN law.

In the upper part of Table 3 for one-proton radioactivity, the predicted half-life for each candidate nucleus is compared with the results obtained from the UDLP systematics and the NGN law. For most cases, the three approaches yield decay half-lives with similar orders of magnitude, demonstrating the stability of the present improved formulation and robust estimations for unmeasured proton emitters. Notably, for nuclei such as $^{117}$Lu$^{m}$ and $^{108}$I, our results agree very well with the available experimental information, indicating the reliability of the present improved GN law for the extrapolations.

The present improved formalism was also applied to two-proton emission candidates. The lower part of Table 3 lists the predicted half-lives for 14 nuclei with non-negative $Q_{2p}$ values extracted from Refs. [50, 51]. A comparison with GLDM, ELDM, the four-parameter empirical formula, and the NGN law shows that the present results exhibit good overall consistency. Because most of these nuclei decay with $l = 0$, the centrifugal contribution is minimal, and the decay systematics are governed primarily by the Coulomb term. The agreement with existing models indicates that the present improved GN law is a reliable tool for extending two-proton decay predictions beyond experimentally explored regions.

## IV. SUMMARY

An improved empirical Geiger–Nuttall (GN) law is developed for the description of both one-proton and two-proton radioactivity by introducing an explicit separation parameter between the Coulomb and centrifugal contributions to the decay half-life. This formulation differs from previous GN-type relations, in which the two contributions are usually treated as a single additive term. The additional degree of freedom provided by the independent coefficient of the angular-momentum term allows the improved GN law to capture the distinct physical roles of the Coulomb and centrifugal potentials. The parameters of the improved GN law for one-proton radioactivity are determined by fitting the experimental half-lives of 44 known emitters. The resulting standard deviation of $\sigma = 0.357$ represents a noticeable improvement over existing empirical relations. The model reproduces the experimental data with high accuracy, which is also reflected by the strong Pearson correlation coefficient obtained from the comparison between theoretical calculations and experimental data. The same formulation applied to established two-proton emitters yields a standard deviation of $\sigma = 0.6728$, which is comparable to the best available

**Table 3.** Comparison of predicted decay half-lives for both one-proton (upper part) and two-proton (lower part) radioactivity with different theoretical models. The symbol $m/n$ associated with the mother nuclei denotes the isomeric state, and $l_{\min}$ is calculated using Eq. (4).

| Nucleus | $Q_p$(MeV) | $l_{min}$ | $\log_{10}T_{1/2}(s)$ | | | |
|---|---|---|---|---|---|---|
| | | | UDLP | NGN | This work | Expt. |
| $^{103}$Sb | 1.469 | 2 | −9.515 | −9.902 | −9.892 | |
| $^{104}$Sb | 0.519 | 2 | 1.278 | 1.890 | 1.993 | > 0.827 [51] |
| $^{105}$Sb | 0.331 | 2 | 7.980 | 9.216 | 9.382 | > 3.049 [51] |
| $^{108}$I | 0.610 | 2 | −0.024 | 0.433 | 0.473 | > 0.556 [51] |
| $^{111}$Cs | 1.820 | 2 | −10.445 | −10.751 | −10.792 | |
| $^{116}$La | 1.091 | 2 | −5.456 | −5.373 | −5.423 | |
| $^{117}$La$^{m}$ | 0.951 [6] | 4 | −2.155 | −2.191 | −1.996 | ≈ −1.989 [51] |
| $^{127}$Pm | 0.922 | 2 | −2.514 | −2.209 | −2.315 | |
| $^{129}$Pm | 0.152 | 3 | 33.398 | 36.533 | 36.425 | |
| $^{137}$Tb | 0.843 | 5 | 2.717 | 2.977 | 1.997 | |
| $^{140}$Ho | 1.103 | 4 | −1.364 | −1.069 | −1.653 | |
| $^{146}$Tm$^{n}$ | 1.144 | 5 | −0.176 | −0.204 | −0.588 | |
| $^{159}$Re | 1.605 | 0 | −6.223 | −6.377 | −7.480 | |
| $^{164}$Ir | 1.576 | 2 | −4.947 | −4.387 | −5.129 | |
| $^{165}$Ir | 1.556 | 0 | −5.455 | −5.593 | −5.443 | |
| $^{169}$Ir$^{m}$ | 0.780 | 5 | 7.404 | 8.088 | 8.113 | |
| $^{171}$Ir$^{m}$ | 0.402 | 5 | 20.396 | 21.952 | 22.031 | |
| $^{169}$Au | 1.947 | 0 | −7.569 | −7.476 | −7.382 | |
| $^{172}$Au | 0.877 | 2 | 3.586 | 3.991 | 3.557 | > 0.146 [51] |
| $^{172}$Au$^{m}$ | 0.627 | 2 | 9.448 | 9.692 | 9.195 | > −0.260 [51] |
| $^{185}$Bi | 1.540 | 5 | −1.019 | −0.721 | −0.828 | |
| $^{185}$Bi$^{n}$ | 1.720 | 6 | −1.161 | −1.502 | −1.356 | |
| $^{211}$Pa | 0.751 | 5 | 12.545 | 13.268 | 12.985 | |

| Nucleus | $Q_{2p}$(MeV) | $l_{min}$ | $\log_{10}T_{1/2}(s)$ | | | | |
|---|---|---|---|---|---|---|---|
| | | | GLDM | ELDM | Four-Para | NGN | This work |
| $^{26}$S | 1.755 | 0 | −14.590 | −13.860 | −12.710 | −14.160 | −14.056 |
| $^{34}$Ca | 1.474 | 0 | −10.710 | −9.910 | −8.650 | −9.930 | −9.735 |
| $^{36}$Sc | 1.993 | 0 | | −11.740 | −10.300 | −11.660 | −11.756 |
| $^{38}$Ti | 2.743 | 0 | −14.270 | −13.560 | −11.930 | −13.350 | −13.721 |
| $^{39}$Ti | 0.758 | 0 | −1.340 | −0.810 | −0.280 | −1.190 | −0.327 |
| $^{40}$V | 1.842 | 0 | | −9.850 | −8.460 | −9.730 | −9.830 |
| $^{42}$Cr | 1.002 | 0 | −2.880 | −2.430 | −1.780 | −2.760 | −2.335 |
| $^{47}$Co | 1.042 | 0 | | −0.110 | 0.210 | −0.690 | −0.471 |
| $^{49}$Ni | 0.492 | 0 | 14.460 | 14.640 | 12.780 | 12.430 | 13.441 |
| $^{56}$Ga | 2.443 | 0 | | −8.000 | −6.420 | −7.610 | −8.239 |
| $^{58}$Ge | 3.732 | 0 | −13.100 | −11.740 | −9.530 | −10.850 | −11.730 |
| $^{59}$Ge | 2.102 | 0 | −6.970 | −5.710 | −4.440 | −5.540 | −6.134 |
| $^{60}$Ge | 0.631 | 0 | 13.550 | 14.620 | 12.400 | 12.040 | 12.376 |
| $^{61}$As | 2.282 | 0 | | −6.120 | −4.740 | −5.850 | −6.544 |

empirical formulas. The explicit separation of Coulomb and centrifugal components enables a clear quantitative analysis of their relative contributions, revealing systematic behaviors consistent with the expected radial dependence of the two potentials. Its capability to distinguish and quantify the Coulomb and centrifugal contributions provides insights into deeper understanding of charged-particle emission from proton-rich nuclei. Furthermore, the present improved GN law has been used to predict half-lives for potential one-proton and two-proton emitters, producing results that are generally consistent with those from widely used empirical models such as UDLP, GLDM, ELDM, and NGN law. These predictions could serve as useful guidance for future experimental investigations near the proton drip line. Despite the very limited available data, especially for the two-proton emissions, the good accuracy is achieved within the present datasets. More experimental data can be incorporated into future dataset to further improve the empirical descriptions of both one-proton and two-proton radioactivity.



## References


[1] K. Jackson, C. Cardinal, H. Evans, N. Jelley, and J. Cerny, Phys. Lett. B **33**, 281 (1970)
[2] J. Cerny, J. Esterl, R. Gough, and R. Sextro, Phys. Lett. B **33**, 284 (1970)
[3] A. Sonzogni, Nucl. Data Sheets **95**, 1 (2002)
[4] D. Delion, R. Liotta, and R. Wyss, Phys. Rev. Lett. **96**, 072501 (2006)
[5] D. Basu, P. Chowdhury, and C. Samanta, Phys. Rev. C **72**, 051601 (2005)
[6] B. Blank and M. Borge, Prog. Part. Nucl. Phys. **60**, 403 (2008)
[7] H. Zhang, Y. Wang, J.-M. Dong, J.-Q. Li, and W. Scheid, J. Phys. G **37**, 085107 (2010)
[8] K. Santhosh and I. Sukumaran, Phys. Rev. C **96**, 034619 (2017)
[9] K. Auranen, A. Briscoe, L. Ferreira, T. Grahn, P. Greenlees, A. Herzáň, A. Illana, D. Joss, H. Joukainen, *et al.*, Phys. Rev. Lett. **128**, 112501 (2022)
[10] Y.-J. Ren and Z.-Z. Ren, Phys. Rev. C **85**, 044608 (2012)
[11] A. I. Budaca, R. Budaca, and I. Silisteanu, Nucl. Phys. A **951**, 60 (2016)
[12] J. Dudek, Z. Szymański, and T. Werner, Phys. Rev. C **23**, 920 (1981)
[13] B. Buck, A. Merchant, and S. Perez, Phys. Rev. C **45**, 1688 (1992)
[14] S. Alavi, V. Dehghani, and M. Sayahi, Nucl. Phys. A **977**, 49 (2018)
[15] M. Bhattacharya and G. Gangopadhyay, Phys. Lett. B **651**, 263 (2007)
[16] A. Zdeb, M. Warda, C. Petrache, and K. Pomorski, Eur. Phys. J. A **52**, 323 (2016)
[17] J.-L. Chen, X.-H. Li, J.-H. Cheng, J.-G. Deng, and X.-J. Wu, J. Phys. G **46**, 065107 (2019)
[18] M. Balasubramaniam and N. Arunachalam, Phys. Rev. C **71**, 014603 (2005)
[19] J.-M. Dong, H.-F. Zhang, W. Zuo, and J.-Q. Li, Chin. Phys. C **34**, 182 (2010)
[20] C. Guo, G. Zhang, and X. Le, Nucl. Phys. A **897**, 54 (2013)
[21] J.-G. Deng, X.-H. Li, J.-L. Chen, J.-H. Cheng, and X.-J. Wu, Eur. Phys. J. A **55**, 58 (2019)
[22] O. Ghodsi and M. Hassanzad, Phys. Rev. C **101**, 034606 (2020)
[23] K.-Y. Zhang, X.-T. He, J. Meng, C. Pan, C.-W. Shen, C. Wang, and S.-Q. Zhang, Phys. Rev. C **104**, L021301 (2021)
[24] P. Zhao, L.-S. Song, B. Sun, H. Geissel, and J. Meng, Phys. Rev. C **86**, 064324 (2012)
[25] Y.-L. Yang, Y.-K. Wang, P. Zhao, and Z.-P. Li, Phys. Rev. C **104**, 054312 (2021)
[26] P. Zhao, Z.-P. Li, J.-M. Yao, and J. Meng, Phys. Rev. C **82**, 054319 (2010)
[27] K.-N. Huang, M. Aoyagi, M. Chen, B. Crasemann, and H. Mark, At. Data Nucl. Data Tables **18**, 243 (1976)
[28] Y.-B. Qian and Z.-Z. Ren, Eur. Phys. J. A **52**, 68 (2016)
[29] Y. Xiao, S.-Z. Xu, R.-Y. Zheng, X.-X. Sun, L.-S. Geng, and S.-S. Zhang, Phys. Lett. B **845**, 138160 (2023)
[30] Q. Lu, K.-Y. Zhang, and S.-S. Zhang, Phys. Lett. B **856**, 138922 (2024)
[31] Z.-Z. Ren, C. Xu, and Z.-J. Wang, Phys. Rev. C **70**, 034304 (2004)
[32] C. Xu and Z.-Z. Ren, Nucl. Phys. A **753**, 174 (2005)
[33] D. Basu, J. Phys. G **30**, B7 (2004)
[34] Y.-B. Qian, Z.-Z. Ren, D.-D. Ni, and Z.-Q. Sheng, Chin. Phys. Lett. **27**, 112301 (2010)
[35] R. Budaca and A. Budaca, Eur. Phys. J. A **53**, 160 (2017)
[36] I. Sreeja and M. Balasubramaniam, Eur. Phys. J. A **54**, 106 (2018)
[37] J.-L. Chen, J.-Y. Xu, J.-G. Deng, X.-H. Li, B. He, and P.-C. Chu, Eur. Phys. J. A **55**, 214 (2019)
[38] L. Grigorenko, R. Johnson, I. Mukha, I. Thompson, and M. Zhukov, Phys. Rev. Lett. **85**, 22 (2000)
[39] L. Grigorenko, R. Johnson, I. Mukha, I. Thompson, and M. Zhukov, Phys. Rev. C **64**, 054002 (2001)
[40] L. Grigorenko and M. Zhukov, Phys. Rev. C **68**, 054005 (2003)
[41] L. Grigorenko and M. Zhukov, Phys. Rev. C **76**, 014008 (2007)
[42] K. Miernik, W. Dominik, Z. Janas, M. Pfützner, L. Grigorenko, C. Bingham, H. Czyrkowski, M. Ćwiok, I. Darby, R. Dąbrowski, *et al.*, Phys. Rev. Lett. **99**, 192501 (2007)
[43] F. Barker, Phys. Rev. C **63**, 047303 (2001)
[44] H.-M. Liu, X. Pan, Y.-T. Zou, J.-L. Chen, J.-H. Cheng, B. He, and X.-H. Li, Chin. Phys. C **45**, 044110 (2021)
[45] M. Gonçalves and S. Duarte, Phys. Rev. C **48**, 2409 (1993)
[46] M. Gonçalves, N. Teruya, O. Tavares, and S. Duarte, Phys. Lett. B **774**, 14 (2017)
[47] J. Cui, Y. Gao, Y. Wang, and J. Gu, Phys. Rev. C **101**, 014301 (2020)
[48] I. Sreeja and M. Balasubramaniam, Eur. Phys. J. A **55**, 33 (2019)
[49] H.-M. Liu, Y.-T. Zou, X. Pan, J.-L. Chen, B. He, and X.-H. Li, Chin. Phys. C **45**, 024108 (2021)
[50] F. Kondev and S. Naimi, Chin. Phys. C **41**, 030003 (2017)
[51] G. Audi, F. Kondev, M. Wang, W. Huang, and S. Naimi, Chin. Phys. C **41**, 030001 (2017)

[52] Y. Xing, Y. Luo, Y. Zhang, M. Wang, X. Zhou, J. Li, K. Li, Q. Yuan, Y. Niu, *et al*., Phys. Rev. Lett. **135**, 012501 (2025)
[53] C. Qi, D. Delion, R. Liotta, and R. Wyss, Phys. Rev. C **85**, 011303 (2012)
[54] S. Duarte and M. Gonçalves, Phys. Rev. C **53**, 2309 (1996)
[55] I. Mukha, K. Sümmerer, L. Acosta, M. Alvarez, E. Casarejos, A. Chatillon, D. Cortina-Gil, J. Espino, A. Fomichev, J. García-Ramos, *et al*., Phys. Rev. Lett. **99**, 182501 (2007)
[56] M. Pfützner, E. Badura, C. Bingham, B. Blank, M. Chartier, H. Geissel, J. Giovinazzo, L. Grigorenko, R. Grzywacz, M. Hellström, *et al*., Eur. Phys. J. A **14**, 279 (2002)
[57] J. Giovinazzo, B. Blank, M. Chartier, S. Czajkowski, A. Fleury, M. Lopez Jimenez, M. Pravikoff, J.-C. Thomas, F. de Oliveira Santos, M. Lewitowicz, *et al*., Phys. Rev. Lett. **89**, 102501 (2002)
[58] L. Audirac, P. Ascher, B. Blank, C. Borcea, B. Brown, G. Canchel, C. Demonchy, F. de Oliveira Santos, C. Dossat, J. Giovinazzo, *et al*., Eur. Phys. J. A **48**, 179 (2012)
[59] C. Dossat, A. Bey, B. Blank, G. Canchel, A. Fleury, J. Giovinazzo, I. Matea, F. de Oliveira Santos, G. Georgiev, S. Grévy, *et al*., Phys. Rev. C **72**, 054315 (2005)
[60] M. Pomorski, M. Pfützner, W. Dominik, R. Grzywacz, A. Stolz, T. Baumann, J. Berryman, H. Czyrkowski, and R. Dabrowski, Phys. Rev. C **90**, 014311 (2014)
[61] B. Blank, A. Bey, G. Canchel, C. Dossat, A. Fleury, J. Giovinazzo, I. Matea, N. Adimi, F. de Oliveira Santos, I. Stefan, *et al*., Phys. Rev. Lett. **94**, 232501 (2005)
[62] P. Ascher, L. Audirac, N. Adimi, B. Blank, C. Borcea, B. Brown, I. Companis, F. Delalee, C. Demonchy, F. de Oliveira Santos, *et al*., Phys. Rev. Lett. **107**, 102502 (2011)
[63] T. Goigoux, P. Ascher, B. Blank, M. Gerbaux, J. Giovinazzo, S. Grévy, T. Kurtukian Nieto, C. Magron, P. Doornenbal, G. Kiss, *et al*., Phys. Rev. Lett. **117**, 162501 (2016)
[64] W. Whaling, Phys. Rev. **150**, 836 (1966)
[65] M. Jager, R. Charity, J. Elson, J. Manfredi, M. Mahzoon, L. Sobotka, M. McCleskey, R. Pizzone, B. Roeder, A. Spiridon, *et al*., Phys. Rev. C **86**, 011304 (2012)
[66] G. Kekelis, M. Zisman, D. Scott, R. Jahn, D. Vieira, J. Cerny, and F. Ajzenberg-Selove, Phys. Rev. C **17**, 1929 (1978)
[67] R. Kryger, A. Azhari, M. Hellström, J. Kelley, T. Kubo, R. Pfaff, E. Ramakrishnan, B. Sherrill, M. Thoennessen, S. Yokoyama, *et al*., Phys. Rev. Lett. **74**, 860 (1995)
[68] D. Suzuki, H. Iwasaki, D. Beaumel, L. Nalpas, E. Pollacco, M. Assié, H. Baba, Y. Blumenfeld, D. De Séréville, A. Drouart, *et al*., Phys. Rev. Lett. **103**, 152503 (2009)
[69] C. Woodward, R. Tribble, and D. Tanner, Phys. Rev. C **27**, 27 (1983)